Molecular Cell, Volume *30*

Supplemental Data

Recurrent Initiation: A Mechanism for Triggering p53 Pulses in Response to DNA Damage

Eric Batchelor, Caroline Mock, Irun Bhan, Alexander Loewer, and Galit Lahav

Supplemental Experimental Procedures

Plasmids and cell lines

To generate the plasmid pMT-p53-Venus (p237) we used MultiSite-Gateway recombination (Invitrogen). Briefly, we amplified the rat metallothionein promoter (pMT) as described in (Lahav et al., 2004), the p53 cDNA and the Venus cDNA individually by PCR with primers containing *attB* sites, and cloned each into pDONR plasmids by recombination (BP clonase, Invitrogen). We then generated a fusion construct by three-fragment recombination (LR Clonase Plus, Invitrogen) using the pDONR plasmids and a modified pDESTR4R3 vector containing a Neomycin selection marker. After transfection in MCF7 cells (FuGene6, Roche) and selection with G418 (0.4 mg/ml), we obtained the clonal cell line of MCF7 expressing p53-Venus by FACS sorting. See **Figure S1** for primer sequences and additional information.

Supplemental References

Lahav, G., Rosenfeld, N., Sigal, A., Geva-Zatorsky, N., Levine, A. J., Elowitz, M. B., and Alon, U. (2004). Dynamics of the p53-Mdm2 feedback loop in individual cells. Nat Genet *36*, 147-150.

Parameter	Description	Value	
β_p	$p53_{inactive}$ production rate	0.9 C_s h^{-1}	0.87 P_{max} h^{-1}
β_{sp}	Saturating production rate of $p53_{active}$	10 h^{-1}	
β_m	p53-dependent Mdm2 production rate	0.9 h^{-1}	1.24 M_{max} P_{max}^{-1} h^{-1}
β_{mi}	p53-independent Mdm2 production rate	0.2 C_s h^{-1}	0.27 M_{max} h^{-1}
β_i	Inhibitor production rate	0.25 h^{-1}	1.03 I_{max} P_{max}^{-1} h^{-1}
β_s	Signal production rate	10 C_s h^{-1}	7.5 S_{max} h^{-1}
α_{mpi}	Mdm2-dependent $p53_{inactive}$ degradation rate	5 C_s^{-1} h^{-1}	3.76 M_{max}^{-1} h^{-1}
α_{pi}	Inactive p53 degradation rate	2 h^{-1}	
α_{mpa}	Mdm2-dependent $p53_{active}$ degradation rate	1.4 C_s^{-1} h^{-1}	1.05 M_{max}^{-1} h^{-1}
α_{sm}	Signal-dependent Mdm2 inactivation rate	0.5 C_s^{-1} h^{-1}	0.67 S_{max}^{-1} h^{-1}
α_m	Mdm2 degradation rate	1 h^{-1}	
α_i	Inhibitor degradation rate	0.7 h^{-1}	
α_{is}	Saturating Inhibitor-dependent Signal degradation rate	50 h^{-1}	
α_s	Inhibitor-independent Signal degradation rate	7.5 h^{-1}	
τ_m	Time delay in Mdm2 production	0.7 h	
τ_i	Time delay in Inhibitor production	1.25 h	
T_s	Signal concentration for half-maximal p53 production	1 C_s	0.75 S_{max}
T_i	Inhibitor concentration for half-maximal Signal degradation	0.2 C_s	0.79 I_{max}
n_s	Hill coefficient of active p53 production by Signal	4	
n_i	Hill coefficient of Signal degradation by Inhibitor	4	
$p53_{inactive0}$	Initial $p53_{inactive}$ concentration	0.3 C_s	0.29 P_{max}
$p53_{active0}$	Initial $p53_{active}$ concentration	0 C_s	0 P_{max}
$Mdm2_0$	Initial Mdm2 concentration	0.2 C_s	0.27 M_{max}
$Inhibitor_0$	Initial Inhibitor concentration	0 C_s	0 I_{max}
$Signal_0$	Initial Signal concentration	0 C_s	0 S_{max}

Table S1. Parameters and initial conditions of the dynamical model. C_s = simulated concentration units. P_{max}, M_{max}, I_{max}, and S_{max} refer to the maximum concentrations of total p53 ($p53_{active}$ + $p53_{inactive}$), Mdm2, Inhibitor, and Signal, respectively, in the simulated response shown in **Figure 5B** of the main text. Where appropriate, we report parameter values in two different units of measurement: simulated concentration units (left column of "Value") and units relative to the maximum concentrations of the five modeled species (right column of "Value").

Figure S1

A

pMT attB4 forward:	GGGGACAACTTTGTATAGAAAAGTTGTAGTGGATCCCGCTGCACTCCG
pMT attB1 reverse:	GGGGACTGCTTTTTTGTACAAACTTGAGATCTGGTGAAGCTGGAGCTAC
p53 attB1 forward:	GGGGACAAGTTTGTACAAAAAAGCAGGCTTCATGGAGGAGCCGCAGTCAG
p53 attB2 reverse:	GGGGACCACTTTGTACAAGAAAGCTGGGTCGTCTGAGTCAGGCCCTTCTGTC
Venus attB2 forward:	GGGGACAGCTTTCTTGTACAAAGTGGGAATGGTGAGCAAGGGCGAGGAG
Venus attB3 reverse:	GGGGACAACTTTGTATAATAAAGTTGCCGGCCGCGAATTAAAAAACC

B

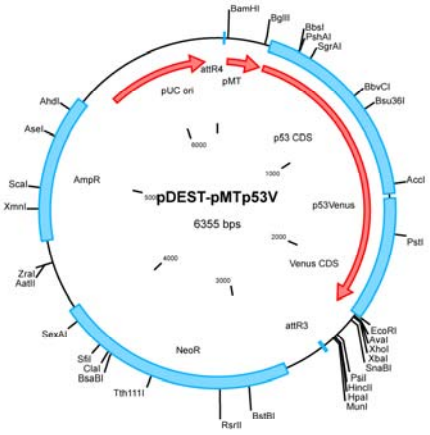

C

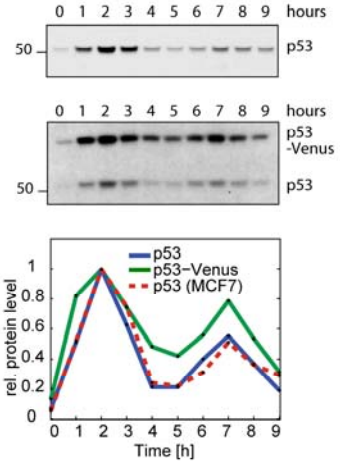

D

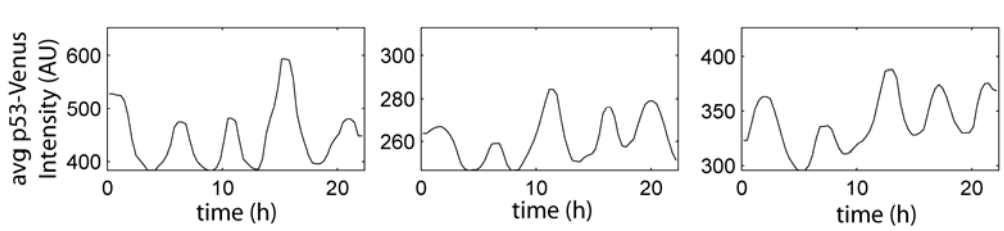

Figure S1. Construction and characterization of MCF7 cells expressing a p53-Venus fusion. (A) Sequences of the oligonucleotides used to clone the construct pMT-p53-Venus (p237). (B) Schematic map of the plasmid pMT-p53-Venus (p237) (C) Western blot analysis showing that the p53-Venus fusion protein follows the dynamics of the endogenous p53 protein. MCF7 cells (top blot) or clonal MCF7 cells expressing p53-Venus (bottom blot) were irradiated with 10 Gy of γ-irradiation and harvested after the indicated time points. Endogenous p53 and the fusion protein were detected using a polyclonal p53 antibody (FL393, Santa Cruz Biotechnology). The graph shows the quantification of the band intensities relative to peak protein level. (D) Average p53-Venus levels in arbitrary units (AU) in three representative clonal MCF7 cells expressing p53-Venus following exposure of cells to 10Gy of γ-irradiation.

Figure S2

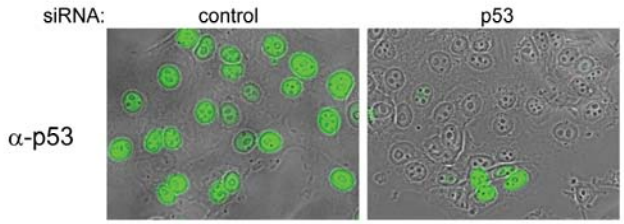

Figure S2. p53 RNAi efficiency. MCF7 cells were transfected with control siRNA or a pool of p53 siRNA. Two days after transfection cells were irradiated with 10 Gy of γ-irradiation, fixed two hours after irradiation, and immunofluorescence was performed to visualize p53 levels as described in Materials and Methods (main text).

Figure S3

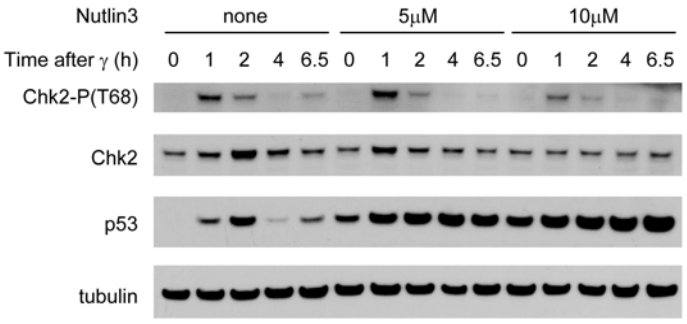

Figure S3. The effect of Nutlin3 on p53 and Chk2. Immunoblots of Chk2-P(T68), total Chk2, and p53 kinetics in MCF7 cells irradiated with 10Gy of γ-irradiation pre-treated without Nutlin3, with 5μM of Nutlin3 (2h pre-treatment), or with 10μM of Nutlin3 (4h pre-treatment).

Figure S4

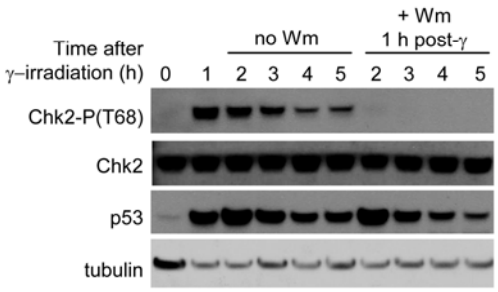

Figure S4. A short induction of ATM-P/Chk2-P is sufficient to drive a full pulse of p53. Immunoblots of Chk2-P(T68) and p53 kinetics in MCF7 cells irradiated with 10Gy of γ-irradiation. Fresh medium containing 100μM wortmannin (+ Wm) or no wortmannin (no Wm) was added to cells 1 h after irradiation. Blots are representative of triplicate experiments.

Figure S5

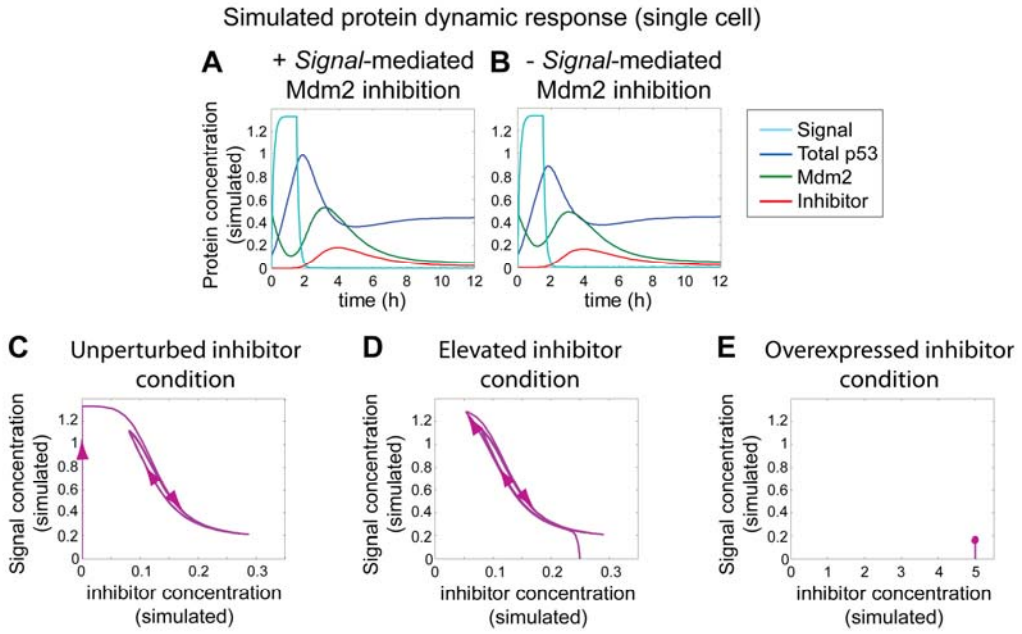

Figure S5. Simulations of Mdm2-mediated *Signal* inhibition and phase plane portraits. (A) The model presented in the main text recapitulates the continued increase in total p53 levels following the inhibition of *Signal* during its initial pulse, as observed in **Figure 4D** (main text). (B) Removal of the term corresponding to *Signal*-mediated Mdm2 inhibition (by setting $\alpha_{sm} = 0$) reduces the increase in p53 levels following *Signal* inhibition. (C-E) Phase plane trajectories of *Signal* concentration versus *inhibitor* concentration obtained from the numerical simulations of the response to γ-irradiation. Simulations correspond to the unperturbed condition (A, corresponding to **Figure 4A** and **4B** of the main text), elevated inhibitor condition (B, corresponding to **Figure 4C** and **4D** of the main text), and overexpressed inhibitor condition (C, corresponding to **Figure 4E** and **4F** of the main text).

Figure S6

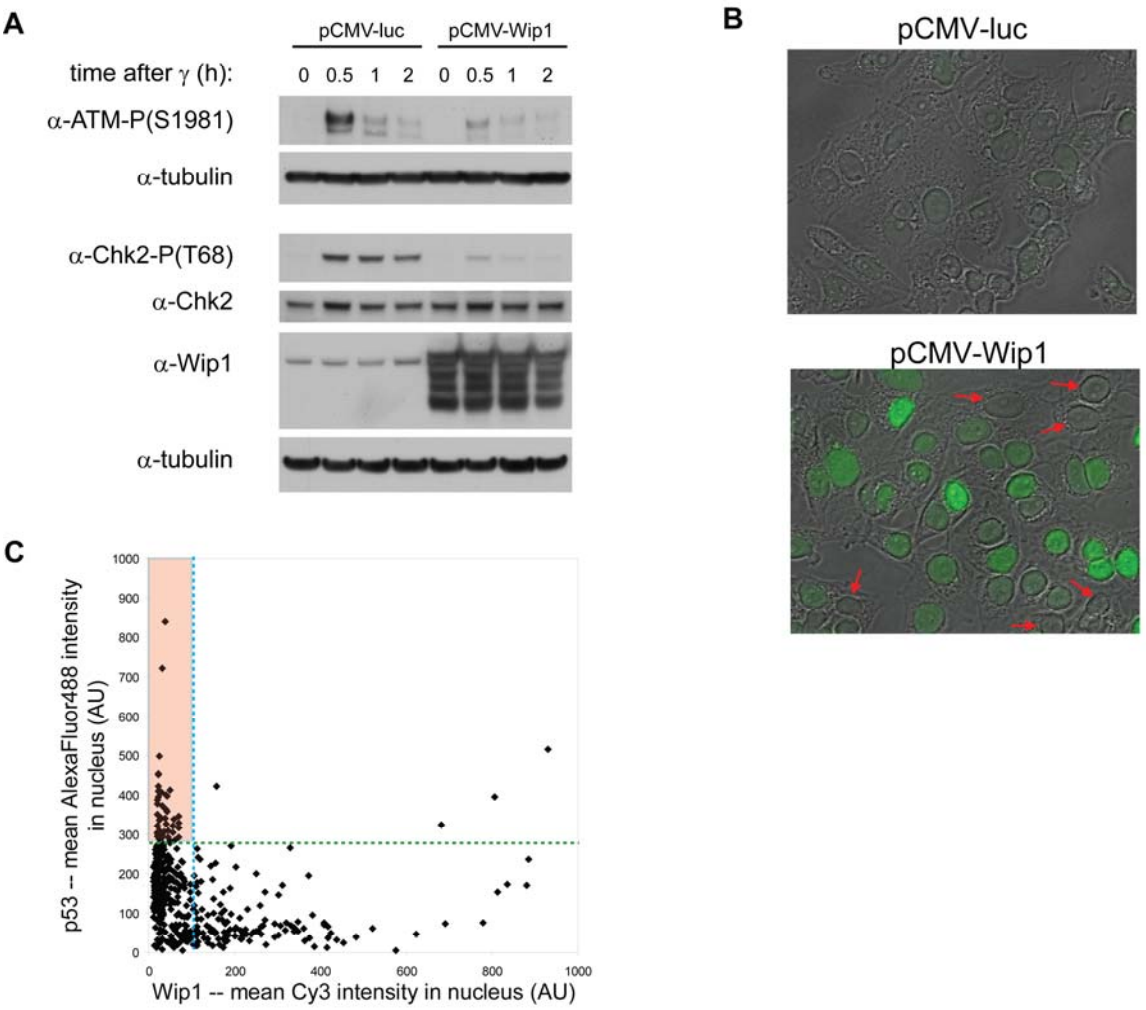

Figure S6. Wip1 overexpression. (A) MCF7 cells were transfected with pCMV-luc or pCMV-Wip1 plasmid DNA. Two days after transfection, cells were treated with 10 Gy γ-irradiation. Cells were harvested at the indicated time points after irradiation, and whole cell lysates were analyzed by Western blot for ATM-P(S1981), Chk2-P(T68), Chk2, and Wip1 levels. (B) MCF7 cells were transfected with pCMV-luc or pCMV-Wip1 plasmid DNA. Two days after transfection, cells were fixed. Immunofluorescence analysis was performed to detect Wip1 levels. Red arrows indicate cells without Wip1 signal. ~74% of unirradiated cells express Wip1 above the background level of the pCMV-luc control cells (n = 484 cells analyzed). (C) MCF7 cells were transfected with pCMV-Wip1 plasmid DNA two days prior to irradiation with 10 Gy γ-irradiation. Cells were fixed two hours later and co-immunofluorescence analysis was performed to detect p53 and Wip1 levels (see Methods, main text). Cells with relatively high p53 expression tended to have low Wip1 expression. Of those cells with a p53 signal greater than the mean + 1SD p53 signal (cells above the dashed green line), ~89% show Wip1 signal that is less than the mean Wip1 signal (cells to the left of the dashed blue line in the shaded region)

Figure S7

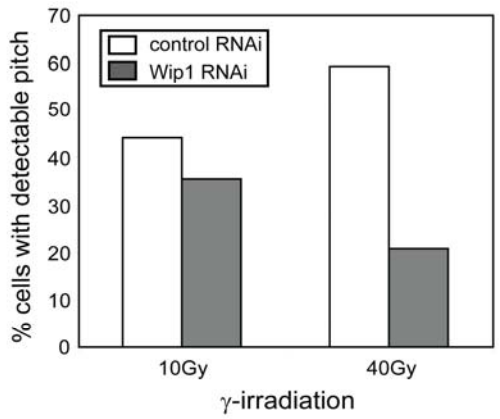

Figure S7. Wip1 RNAi reduces the regularity of p53 pulses. Pitch analysis as described in Geva-Zatorsky *et al.*, 2006, using a sliding window of 32 points, was performed on the p53-Venus signals from the single-cell experiments shown in **Figure 6** (main text). The plot shows the percentage of cells with a detectable pitch, which we define as those cells with an autocorrelation greater than 0.

Figure S8

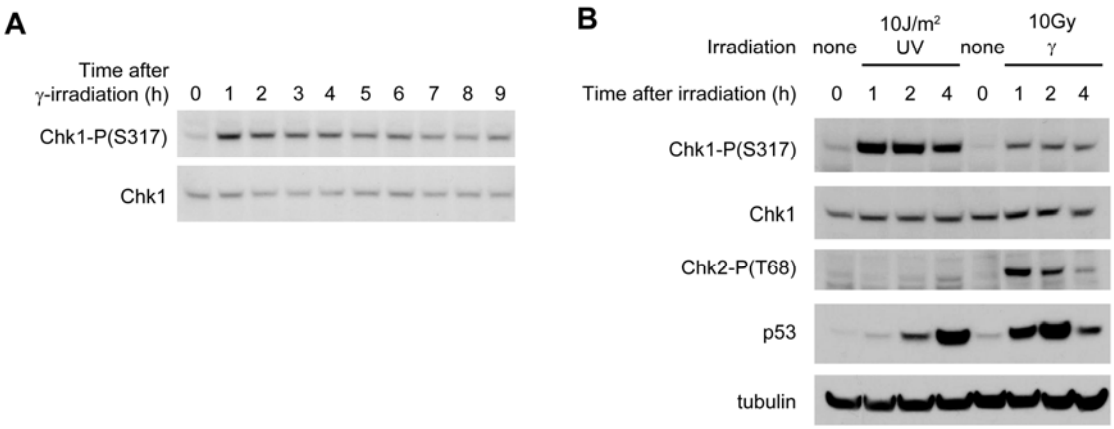

Figure S8. Chk1-P does not show pulses of activity in response to γ-irradiation. (A) Immunoblots of Chk1-P(S317) and total Chk1 kinetics in MCF7 cells irradiated with 10Gy of γ-irradiation. (B) Immunoblots of Chk1-P(S317), Chk2-P(T68), and p53 kinetics in MCF7 cells treatted with 10J/m^2 of UV-irradiation or 10Gy of γ-irradiation.

Figure S9

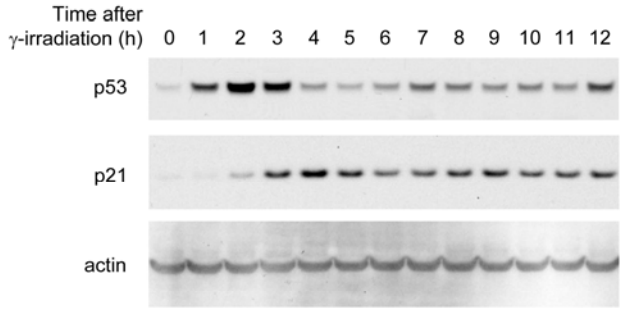

Figure S9. p21 pulses follow p53 pulses in response to γ-irradiation. Immunoblots of p53 and p21 kinetics in MCF7 cells irradiated with 10Gy of γ-irradiation. Blots are representative of triplicate experiments.